

Effects of Mutual Coupling on Lattice Reduction-Aided Millimeter Wave Hybrid Beamforming

Denisa Prisiceanu*, K. Satyanarayana*, Mohammed El-Hajjar*, Ping-Heng Kuo[†], Alain Mourad[†], Lajos Hanzo*

*Department of Electronics and Computer Science, University of Southampton, UK.

[†]InterDigital Europe Ltd., London, UK.

Email: {ks1r15, meh, lh}@ecs.soton.ac.uk, {ping-heng.kuo, alain.mourad}@InterDigital.com

Abstract—Millimeter wave (mmWave) communications has gained considerable attention due to the availability of large bandwidths, which can be harnessed to meet the ever-increasing data rate demands. Directional beamforming combined with baseband precoding should be used owing to the high propagation losses encountered at mmWave frequencies. This is typically referred to as hybrid beamforming. In hybrid beamforming arrangements, the adjacent antenna elements are closely spaced, typically at half-wavelength spacing in order to compensate for the propagation losses. In this antenna array configuration, the mutual coupling between the adjacent antenna elements becomes significant and may limit the performance of the system. Therefore, in this paper, we propose a reduced-complexity near-optimal detection scheme, namely the so-called Element-based Lattice Reduction algorithm, for hybrid beamforming in mmWave communications and we investigate its performance in the presence of mutual coupling. We demonstrate that the mutual coupling affects the spatial correlation of the channels between the different antennas depending on the distance between the antenna elements, which has a direct effect on the achievable rate as well as bit error ratio (BER) performance of the system.

Index Terms—Hybrid beamforming, Lattice Reduction, mmWave communications.

I. INTRODUCTION

There is a dearth of spectral resources in the sub-6 GHz frequency band due to the escalating data rate demands of users. Hence, harnessing the hitherto unused bandwidth available at millimeter wave (mmWave) frequencies is an attractive solution to yield satisfactory data rates [1]. However, migrating from communications in the microwave frequencies to the mmWave frequencies imposes numerous challenges. More explicitly, mmWave frequencies experience high propagation losses because of the attenuation due to oxygen absorption, rain-induced fading and foliage density, which has detrimental effects on the signal-to-noise ratio (SNR) at the receiver [2], [3]. Hence, in order to compensate for the propagation losses, high-gain directional transmission has to be employed, which is termed as beamforming [4] and typically relies on spacing the antenna elements at half wavelength distance [2]. Given that the wavelength at mmWave frequencies is on the order of millimeters, large number of antennas can be packed in a compact area to attain massive beamforming gains.

Traditionally, in digital beamforming a separate radio frequency (RF) chain, including the digital-to-analog and analog-to-digital converters (DAC/ADC), is dedicated to every antenna element of the antenna array. However, in mmWave communications, since large antenna arrays are installed to obtain satisfactory beamforming gains, dedicating a separate RF chain to every antenna element would incur both excessive hardware complexity and high power consumption [4]. To circumvent this challenge, a hybrid beamforming scheme was proposed [5], where beamforming is carried out in two stages: at the

RF stage using analog phase-shifters and in the baseband using digital processing. In hybrid beamforming, the signals are first digitally processed in the baseband using a digital transmit precoder (TPC) and then the precoded signals are upconverted and phase shifted in the RF stage, before they are fed to the transmit antennas. It is instructive to note that in hybrid beamforming the number of DACs/ADCs used for digital processing is typically lower than the number of phase shifters used in the RF. Employing analog phase shifters in the RF stage has its own limitations such as the angular resolution, which is typically not accurate [4]. However, the errors introduced by the analog beamformer are mitigated by the ensuing digital processing in the baseband using TPC [5]. The state-of-the art hybrid beamforming architectures includes the so-called fully-connected and sub-array-connected design [6]. In fully-connected design, the signals generated after digital processing by the TPC are sent to the phase-shifters that are connected to all the transmit antennas. By contrast, in the sub-array-connected design, the phase-shifters are connected to only a subset of the transmit antennas. More recently, we proposed a dual-function hybrid beamforming architecture in [7], [8], where both beamforming and diversity gains can be achieved.

In the literature, most of the work is focused on designing the precoders and combiners for the aforementioned designs. El Ayach *et al.* [9] proposed a hybrid precoding relying on algorithm referred to as orthogonal matching pursuit (OMP). As a further solution, Song *et al.* [10] proposed a codebook design for mmWave systems using the OMP scheme. Sohrabi *et al.* [11] discussed a hybrid precoding solution based on the algorithm proposed by Pi in [12]. Several other treatises [13], [14] were focused on the codebook design for mmWave hybrid beamforming systems.

However, these contributions do not consider the mutual coupling effects between the adjacent antenna elements of the array. Since the antennas are closely spaced, the mutual coupling between the antennas becomes significant and this may limit the system's performance in practice. When the antenna elements are closely spaced, the radiation of each antenna element affects the radiation pattern of the other antennas, which in turn affects the input impedance of the antenna elements. This phenomenon is termed as mutual coupling. Mutual coupling may limit the system's performance in practice, since the radiation efficiency of the antennas is reduced because of the radiation from closely-spaced antenna elements. Gupta *et al.* [15] advocated that the mutual coupling can bring detrimental effects on the system performance. However, there is paucity of work focused on analysing the

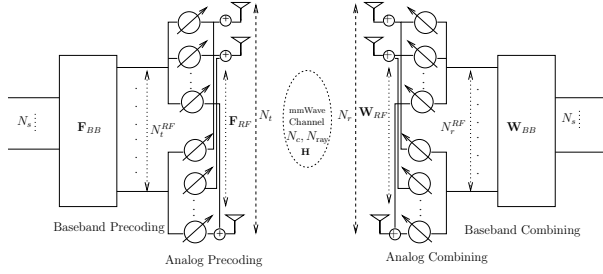


Fig. 1. Hybrid beamforming transceiver architecture.

effect of mutual coupling in hybrid beamforming systems. In [16], the authors analyzed the mutual coupling effects on the channel capacity. More recently, Liu *et al.* [17] investigated the impact of mutual coupling on the capacity of antenna arrays.

Against this background, in this paper we investigate the performance of hybrid beamforming system in the face of mutual coupling relying on a practical codebook using discrete Fourier transform (DFT) and mutually unbiased bases (MUB) precoders of [8]. Furthermore, we employ an Element-based Lattice Reduction (ELR)-aided decoder at the receiver [18], [19], which performs close to the maximum-likelihood (ML) detector at a significantly lower complexity [20]. Although there are other state-of-the-art lattice reduction techniques, such as the Lenstra, Lanstra, and Lovasz (LLL) algorithm [21], and the Korkine-Zolotareff (KZ) algorithm [22], ELR assisted detection significantly reduces the complexity when large-scale MIMOs are employed. Additionally, since mmWave communications relies on large-scale yet-compact MIMO, using ELR assisted detection can be an attractive choice.

The rest of the paper is organized as follows. In Section II we introduce the system model followed by the design of the hybrid precoding and combining using ELR-aided decoding in Section III. In Section IV we present our simulation results for characterising the proposed system and finally we conclude in Section V.

Notations: We use upper case boldface, \mathbf{A} , for matrices and lower case boldface, \mathbf{a} , for vectors. We use \mathcal{CN} , \mathcal{U} , and i.i.d. to denote complex-valued normal distribution, uniform distribution, and independent and identical distribution, respectively.

II. SYSTEM MODEL

In this paper we consider the point-to-point single-user mmWave MIMO system shown in Fig. 1, where the transmitter is equipped with N_t antennas and the receiver with N_r antennas. Furthermore, the transmitter and the receiver are equipped with N_t^{RF} and N_r^{RF} chains, respectively. The transmitter then transmits a signal vector \mathbf{s} of dimension N_s and then employs digital precoding to the modulated data using matrix \mathbf{F}_{BB} of size $N_t^{\text{RF}} \times N_s$, as shown in Figure 1. This is then followed by RF beamforming using matrix \mathbf{F}_{RF} of size $N_t \times N_t^{\text{RF}}$. After transmission over the wireless mmWave channel, the receiver performs RF combining using \mathbf{W}_{RF}^H of size $N_r^{\text{RF}} \times N_r$ and then digital combining using \mathbf{W}_{BB}^H . Then the received signal vector \mathbf{y} at the receiver is given by:

$$\mathbf{y} = \sqrt{P} \mathbf{W}_{\text{BB}}^H \mathbf{W}_{\text{RF}}^H \mathbf{H} \mathbf{C} \mathbf{F}_{\text{RF}} \mathbf{F}_{\text{BB}} \mathbf{s} + \mathbf{W}_{\text{BB}}^H \mathbf{W}_{\text{RF}}^H \mathbf{n}, \quad (1)$$

where \mathbf{H} is the statistical channel model expressed as [23]:

$$\mathbf{H} = \sqrt{\frac{N_r N_t}{N_c N_{\text{ray}}}} \sum_{n_c=1}^{N_c} \sum_{n_{\text{ray}}=1}^{N_{\text{ray}}} \alpha_{n_c}^{\text{ray}} \mathbf{a}_r(\phi_{n_c}^{\text{ray}}) \mathbf{a}_t^T(\phi_{n_c}^{\text{ray}}).$$

To elaborate further, \mathbf{H} is the statistical channel matrix of size $N_r \times N_t$ so that $\mathbb{E}[\|\mathbf{H}\|_F^2] = N_t N_r$, while $\alpha_{n_c}^{\text{ray}} \sim \mathcal{CN}(0, 1)$ is a complex-valued Gaussian random variable, whose amplitude and phase are Rayleigh and uniformly distributed, respectively. Furthermore, \mathbf{C} is the mutual coupling matrix at the transmitter of size $N_t \times N_t$, which is described later in this section, whilst \mathbf{n} is the noise vector of i.i.d. entries with distribution $\mathcal{CN}(0, \sigma^2)$. For a uniform linear array (ULA) with N_r and N_t antenna elements, the response vectors \mathbf{a}_r and \mathbf{a}_t are expressed as:

$$\begin{aligned} \mathbf{a}_r(\phi_r) &= [1 \ e^{j \frac{2\pi}{\lambda} d \cos(\phi_r)} \dots e^{j \frac{2\pi}{\lambda} (N_r-1) d \cos(\phi_r)}]^T, \\ \mathbf{a}_t(\phi_t) &= [1 \ e^{j \frac{2\pi}{\lambda} d \cos(\phi_t)} \dots e^{j \frac{2\pi}{\lambda} (N_t-1) d \cos(\phi_t)}]^T. \end{aligned}$$

Finally, N_c and N_{ray} are the number of channel impulse response (CIR) clusters and rays, respectively. It is instructive to note that to employ 3D beamforming, the response vectors $\mathbf{a}_r, \mathbf{a}_t$ can be extended to uniform planar arrays (UPA) as a function of the elevation angle.

Furthermore, since the antenna elements are closely spaced, the radiation of one antenna element affects the impedance of other elements, which results in mutual coupling [24]. The mutual coupling matrix \mathbf{C} of an antenna array is given by [24]:

$$\mathbf{C} = (Z_A + Z_T) (\mathbf{Z} + Z_T \mathbf{I}_{N_t})^{-1},$$

where Z_T is the load impedance and Z_A is the antenna impedance. The mutual impedance matrix \mathbf{Z} is given by [24]:

$$\begin{pmatrix} Z_A + Z_T & Z_{12} & \dots & Z_{1N_t} \\ Z_{21} & Z_A + Z_T & \dots & Z_{2N_t} \\ \vdots & \vdots & \dots & \vdots \\ Z_{N_t1} & Z_{N_t2} & \dots & Z_{N_tN_t} \end{pmatrix}.$$

For a side-by-side wire dipoles with length l , the expression for Z_{mn} is given by [24]:

$$\begin{aligned} Z_{mn} &= 30[2C_i(u_o) - C_i(u_1) - C_i(u_2)] \\ &\quad - j[30(2S_i(u_o) - S_i(u_1) - S_i(u_2))], \end{aligned}$$

where u_o, u_1 , and u_2 are calculated as

$$\begin{aligned} u_o &= \kappa d_h \\ u_1 &= \kappa(\sqrt{d_h^2 + l^2} + l) \\ u_2 &= \kappa(\sqrt{d_h^2 + l^2} - l), \end{aligned}$$

where κ is the wavenumber variable equal to $2\pi/\lambda$, while C_i and S_i are cosine and sine integrals given by [24]

$$\begin{aligned} C_i &= \int_0^u \left(\frac{\cos(x)}{x} \right) dx \\ S_i &= \int_0^u \left(\frac{\sin(x)}{x} \right) dx. \end{aligned}$$

The value of the antenna impedance Z_A for a half-wavelength dipole is equal to $73 + j42.5 \ [\Omega]$, while the load impedance Z_T is typically set to the conjugate of the antenna impedance so as to obtain the impedance match, i.e. $Z_T = Z_A^*$ [24].

For the system model considered in (1), the achievable rate, R , is given by

$$\begin{aligned} R &= \log_2 \det(\mathbf{I}_{N_s} + \\ &\quad \frac{P}{N_s} \mathbf{R}_n^{-1} \mathbf{W}_{\text{BB}}^H \mathbf{W}_{\text{RF}}^H \mathbf{H} \mathbf{C} \mathbf{F}_{\text{RF}} \mathbf{F}_{\text{BB}} \mathbf{F}_{\text{BB}}^H \mathbf{F}_{\text{RF}}^H \mathbf{C}^H \mathbf{H}^H \mathbf{W}_{\text{RF}} \mathbf{W}_{\text{BB}}), \end{aligned} \quad (2)$$

where $\mathbf{R}_n = \sigma^2 \mathbf{W}_{\text{BB}}^H \mathbf{W}_{\text{RF}}^H \mathbf{W}_{\text{RF}} \mathbf{W}_{\text{BB}}$ and P is the signal power.

III. DESIGN OF HYBRID PRECODING AND COMBINING

In this section, we discuss the analog RF beamformer/combiner and digital baseband precoder/combiner employed in this paper, where we choose the RF beamformer/combiner from the discrete Fourier transform (DFT) matrix and the digital baseband precoder from the mutually unbiased bases (MUB) codebook [8], while the digital baseband combiner relies on ELR-aided zero-forcing (ZF) detection.

A. Analog RF Beamforming

The analog RF beamformer matrices \mathbf{F}_{RF} and \mathbf{W}_{RF} at the transmitter and receiver, respectively, are chosen such that the magnitude of each entry in the matrix is constant, which otherwise would increase the complexity as well as cause power imbalance in the system. Hence, we employ a DFT assisted beamformer, where the columns of the DFT vectors are chosen as the beamformer matrix. The columns of the DFT matrix that exhibit maximum correlation with the right singular vectors of the channel matrix, i.e. with \mathbf{V} of $\mathbf{H} = \mathbf{U}\Sigma\mathbf{V}^H$, are selected for the beamforming [8]. More explicitly, we select the N_t^{RF} columns of the RF beamformer \mathbf{F}_{RF} from the DFT matrix as follows

$$\mathbf{F}_{\text{RF}}(:, j) = \max_i \langle \text{DFT}_{N_t}(:, i), \mathbf{V} \rangle, \\ i = 1, \dots, N_t, 1 \leq j \leq N_t^{\text{RF}},$$

where $\langle \cdot \rangle$ denotes the inner product. Similarly, the analog RF combiner matrix is formed from the columns of the DFT matrix, which exhibit maximum correlation with the left singular vectors of the channel matrix, i.e. with \mathbf{U} of $\mathbf{H} = \mathbf{U}\Sigma\mathbf{V}^H$. In other words, we select the N_r^{RF} columns of the RF beamformer \mathbf{W}_{RF} from the DFT matrix as follows

$$\mathbf{W}_{\text{RF}}(:, j) = \max_i \langle \text{DFT}_{N_r}(:, i), \mathbf{U} \rangle, \\ i = 1, \dots, N_r, 1 \leq j \leq N_r^{\text{RF}}.$$

The rationale for selecting the DFT matrix as the RF beamformer is because the column vectors of the DFT matrix match the statistical distribution of the optimal precoder matrix¹.

B. Digital Baseband Precoder

Having designed the analog RF beamformer/combiner, we design the digital baseband precoder using the effective channel matrix $\mathbf{H}_{\text{eff}} = \mathbf{W}_{\text{RF}}^H \mathbf{H} \mathbf{F}_{\text{RF}}$. In this paper, we opted for the digital baseband precoder matrix relying on the codebook constructed from the MUBs [8]. The rationale of selecting the precoder from the MUB assisted codebook is the fact that it strikes a performance versus complexity trade-off. Moreover, the entries of the MUB codebook are constructed from a finite alphabet with unit magnitude, which mitigates the power imbalances in the system. Considering the practical constraints on codebook design as detailed in [25], the MUB codebook constitutes an attractive practical solution. The digital TPC is selected from the MUB codebook \mathcal{F} as follows [8]

$$\mathbf{F}_{\text{BB}} = \arg \max_{\mathbf{F}_{\text{BB}} \in \mathcal{F}} \Lambda_{\min} \{ \mathbf{H}_{\text{eff}} \mathbf{F}_{\text{BB}} \} \quad (3)$$

where Λ_{\min} is the minimum singular value of $\{ \mathbf{H}_{\text{eff}} \mathbf{F}_{\text{BB}} \}$. The step-by-step procedure for constructing the MUB codebook is detailed in [9].

¹The optimal precoder matrix is the right singular vector of the channel matrix.

C. Digital Baseband Combiner

Following the RF combining at the receiver, the receiver will have to employ digital decoding in order to recover the transmitted signals. Based on (1), we can represent the received signal after RF combining as:

$$\mathbf{y} = \sqrt{P} \mathbf{W}_{\text{RF}}^H \mathbf{H} \mathbf{C} \mathbf{F}_{\text{RF}} \mathbf{F}_{\text{BB}} \mathbf{s} + \mathbf{W}_{\text{RF}}^H \mathbf{n}, \\ = \mathbf{H}_{\text{eff,RF}} \mathbf{s} + \mathbf{W}_{\text{RF}}^H \mathbf{n},$$

where $\mathbf{H}_{\text{eff,RF}}$ represents the effective channel after RF combining and before the digital decoding. The optimal decoder is the ML decoder, which searches through all possible constellation points of the transmitted symbol vector \mathbf{x} within the lattice $\mathbf{H}_{\text{eff,RF}} \mathbf{s}$. The ML detection requires complex computations, especially for a large number of antennas. Therefore, to reduce the decoding complexity LR-aided detectors were proposed in [20], [26], which aim to reduce the basis of the lattice $\mathbf{H}_{\text{eff,RF}} \mathbf{s}$ and find another basis having better properties for detection [27]. The LR operation transforms the channel matrix $\mathbf{H}_{\text{eff,RF}}$ into its equivalent channel matrix $\tilde{\mathbf{H}}_{\text{eff,RF}}$, which is more orthogonal and better conditioned than $\mathbf{H}_{\text{eff,RF}}$ [28]. The LR-aided detector uses the new orthogonal channel matrix $\tilde{\mathbf{H}}_{\text{eff,RF}}$, which may give more reliable estimation for the received signal. Therefore, to achieve near-optimal detection in our proposed mmWave system, we perform the digital baseband combining relying on an ELR-aided ZF detector. In this case, after obtaining $\tilde{\mathbf{H}}_{\text{eff,RF}}$ using the ELR algorithm, the conventional ZF detection is performed, where the equalisation matrix \mathbf{W}_{BB} is obtained as the inverse of the new channel matrix $\tilde{\mathbf{H}}_{\text{eff,RF}}$, i.e. $\mathbf{W}_{\text{BB}} = \tilde{\mathbf{H}}_{\text{eff,RF}}^{-1}$.

IV. SIMULATION RESULTS

In this section, we characterise the achievable rate and the BER performance of the proposed system in the presence of mutual coupling. The simulation parameters used in this paper are listed in Table I.

TABLE I
SIMULATION PARAMETERS.

Parameters	Values
N_c	4
N_{ray}	6
N_t	64, 8
N_r	32, 8
N_t^{RF}	4
N_r^{RF}	2
$\phi_{n_c}^{n_{\text{ray}}}$	$\sim \mathcal{U}[0, 2\pi)$

Fig. 2 shows the achievable rate performance of the DFT-MUB hybrid precoding [8] and of the optimally unconstrained precoding, where the precoder matrix is chosen as the right singular vectors and the combiner as the left singular vectors of the channel matrix \mathbf{H} relying on singular value decomposition (SVD). Furthermore, the unconstrained precoding is fully-digital precoder relying on a simplifying assumption of having perfect channel state information. In Fig. 2, a 64×32 MIMO is used, where two spatial streams are transmitted using four RF chains. It can be seen in Fig. 2 (a) and (b) that the mutual coupling degrades the achievable rate of the system employing antenna spacing of 2λ and $\lambda/2$. On the other hand, when the spacing between the adjacent antenna elements is $\lambda/4$ as in Fig. 2 (c), the achievable rate of the system considering mutual

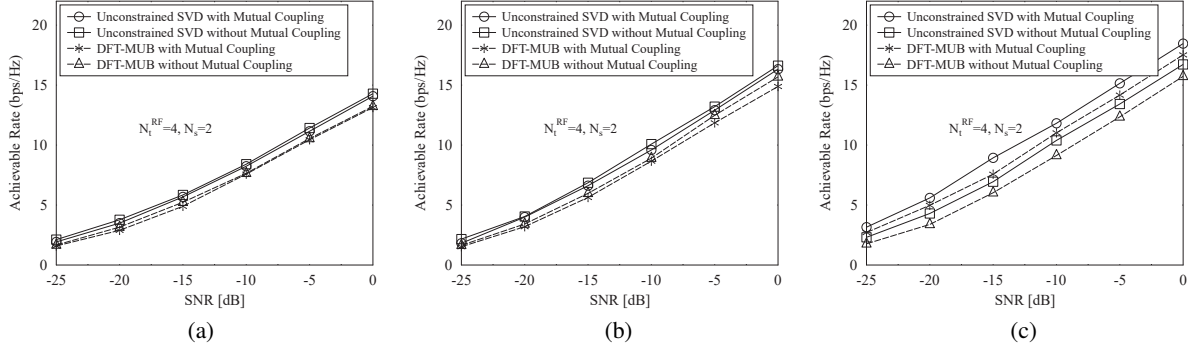


Fig. 2. Achievable rate of the unconstrained precoding and of the DFT-MUB hybrid precoding both with and without mutual coupling for a 64×32 MIMO system. In this setting, two spatial streams are transmitted using four RF chains when (a) the spacing between the adjacent antenna is set to 2λ , (b) the spacing between the adjacent antenna is set to $\lambda/2$, (c) the spacing between the adjacent antenna is set to $\lambda/4$.

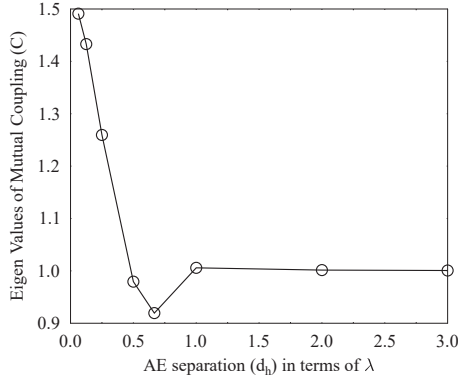


Fig. 3. Eigenvalues of the mutual coupling matrix \mathbf{C} versus the antenna element (AE) separation distance.

coupling becomes better than that without mutual coupling. The capacity gain attained by reducing the antenna spacing to $\lambda/4$ is due to the de-correlation effect introduced by the mutual coupling. It is instructive to note that mutual coupling also affects the received power, where it has been shown in [29] that the achievable rate is more influenced by the de-correlation effect for small antenna spacings.

To elaborate further, let us denote $\mathbf{F}_{\text{RF}}\mathbf{F}_{\text{BB}} = \mathbf{F}$ and $\mathbf{W}_{\text{RF}}\mathbf{W}_{\text{BB}} = \mathbf{W}$. Then, the achievable rate equation of (2) at high SNR can be written as [7]:

$$R = \log_2 \det \left(\frac{P}{N_s} \mathbf{R}_n^{-1} \mathbf{W}^H \mathbf{H} \mathbf{C} \mathbf{F} \mathbf{F}^H \mathbf{C}^H \mathbf{H}^H \mathbf{W} \right), \quad (4)$$

which can be written in terms of the rate without mutual coupling R_{nc} plus the difference due to the mutual coupling as:

$$R = R_{nc} + \log_2 \det (\mathbf{C} \mathbf{C}^H). \quad (5)$$

Furthermore, since $\det (\mathbf{C} \mathbf{C}^H) = \prod_{i=1}^{N_t} c_i$, where c_i represent the eigenvalues of the mutual coupling matrix (\mathbf{C}), the achievable rate depends on the eigenvalues of \mathbf{C} . Fig. 3 shows the eigenvalues of the mutual coupling matrix \mathbf{C} versus the antenna separation distance, where it is shown that for distances less than $\lambda/2$ the eigenvalues are greater than 1, which means that $\log_2 \det (\mathbf{C} \mathbf{C}^H) > 0$ and hence the rate achieved with mutual coupling is greater than that of without mutual coupling as seen in Fig. 2 (c). On the other hand for distances between $\lambda/2$ -to- λ , the eigenvalues are less than one,

which means that the rate achieved with mutual coupling is less than that of without mutual coupling, as seen in Fig. 2 (a) and (b).

Finally, in order to understand the effect of mutual coupling on the system performance, we simulated the BER performance of the system employing the ELR-aided ZF decoding. Fig. 4 shows the BER performance for a 8×8 MIMO, where two 4-QAM symbols are transmitted using four RF chains. More explicitly, Fig. 4 (a) shows the performance of the system employing DFT-MUB with zero-forcing (ZF) and ELR-aided ZF decoder. It can be seen from the Fig. 4 that the ELR-aided ZF decoding significantly improves the system performance compared with the ZF decoder. There is around 5 dB gain at the BER of 10^{-4} . Furthermore, when the mutual coupling is considered, the BER performance of the system employing both decoders degrade, when the spacing between the adjacent antenna elements is $\lambda/2$, as shown in Fig. 4(a). In Fig. 4(b) we plot the BER performance of the system employing ELR-aided ZF with different antenna spacing in the presence of mutual coupling. As shown in Fig. 4 (b), the performance of the system employing $\lambda/4$ antenna spacing is worse than that employing $\lambda/2$ spacing when no mutual coupling is considered. This is expected due to the higher channel spatial correlation at $\lambda/4$ separation. On the other hand, when considering mutual coupling, we observe in Fig. 4 (b) that the performance of the system employing $\lambda/4$ antenna separation is now better than that for the system with $\lambda/2$, which is due to the decorrelation effect of the mutual coupling, which can be observed from Fig. 3.

V. CONCLUSION

In this paper, we investigated the performance of the DFT-MUB hybrid beamforming system in the presence of mutual coupling, when ELR-aided ZF decoding is employed. We demonstrated that the BER as well as the achievable rate performance varies with the spacing between the antenna elements, which is due to the decorrelation effect of the mutual coupling, which varies at different antenna separation distances.

REFERENCES

- [1] A. Ghosh, R. Ratasuk, B. Mondal, N. Mangalvedhe, and T. Thomas, "LTE-advanced: next-generation wireless broadband technology," *IEEE Wireless Commun.*, vol. 17, no. 3, pp. 10–22, June 2010.

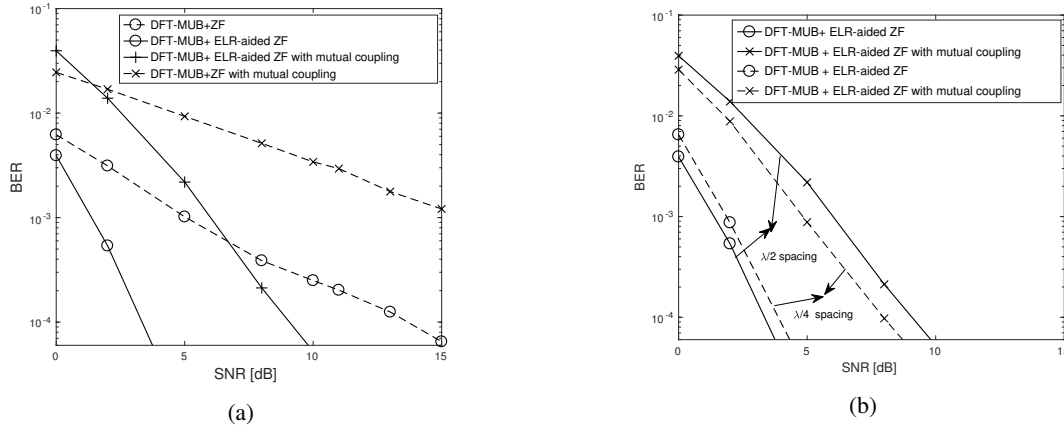


Fig. 4. BER performance of the DFT-MUB with ZF and of DFT-MUB with ELR-aided ZF decoder for a 8×8 MIMO system. In this setting, two spatial streams are transmitted using four RF chains. (a) shows a comparison of the BER performance with ZF and ELR-aided ZF decoders when the spacing between the adjacent antennas is set to $\lambda/2$ and (b) shows a comparison of the BER performance for the system employing ELR-aided ZF decoding when the antenna spacing is varied from $\lambda/2$ to $\lambda/4$.

- [2] I. Hemadeh, K. Satyanarayana, M. El-Hajjar, and L. Hanzo, "Millimeter-wave communications: Physical channel models, design considerations, antenna constructions, and link-budget," *IEEE Commun. Surveys Tuts.*, IEEE Xplore Early Access, 2018.
- [3] S. Rangan, T. S. Rappaport, and E. Erkip, "Millimeter-wave cellular wireless networks: Potentials and challenges," in *Proc. of IEEE*, vol. 102, no. 3, pp. 366–385, March 2014.
- [4] Y. Niu, Y. Li, D. Jin, L. Su, and A. V. Vasilakos, "A survey of millimeter wave (mmwave) communications for 5G: Opportunities and challenges," *CoRR*, vol. abs/1502.07228, 2015. [Online]. Available: <http://arxiv.org/abs/1502.07228>
- [5] X. Zhang, A. F. Molisch, and S.-Y. Kung, "Variable-phase-shift-based RF-baseband codesign for MIMO antenna selection," *IEEE Trans. Signal Process.*, vol. 53, no. 11, pp. 4091–4103, Nov 2005.
- [6] S. Han, Z. Xu, and C. Rowell, "Large-scale antenna systems with hybrid analog and digital beamforming for millimeter wave 5G," *IEEE Commun. Mag.*, vol. 53, no. 1, pp. 186–194, January 2015.
- [7] K. Satyanarayana, M. El-Hajjar, P. H. Kuo, A. Mourad, and L. Hanzo, "Dual-function hybrid beamforming and transmit diversity aided millimeter wave architecture," *IEEE Trans. Veh. Technol.*, vol. PP, no. 99, pp. 1–1, 2017.
- [8] K. Satyanarayana, M. El-Hajjar, P.-H. Kuo, A. Mourad, and L. Hanzo, "Millimeter wave hybrid beamforming with DFT-MUB aided precoder codebook design," in *Proc. VTC (Fall)*, Sept. 2017, pp. 1–5.
- [9] O. El Ayach, S. Rajagopal, S. Abu-Surra, Z. Pi, and R. Heath, "Spatially sparse precoding in millimeter wave MIMO systems," *IEEE Trans. Wireless Commun.*, vol. 13, no. 3, pp. 1499–1513, March 2014.
- [10] J. Song, J. Choi, and D. J. Love, "Codebook design for hybrid beamforming in millimeter wave systems," in *Proc. ICC*, June 2015.
- [11] F. Sofrabi and W. Yu, "Hybrid digital and analog beamforming design for large-scale MIMO systems," in *Proc. ICASSP*, April 2015, pp. 2929–2933.
- [12] Z. Pi, "Optimal transmitter beamforming with per-antenna power constraints," in *Proc. ICC*, June 2012, pp. 3779–3784.
- [13] A. Alkhateeb, G. Leus, and R. W. Heath, "Limited feedback hybrid precoding for multi-user millimeter wave systems," *IEEE Trans. Wireless Commun.*, vol. 14, no. 11, pp. 6481–6494, Nov 2015.
- [14] A. Alkhateeb and R. W. Heath, "Frequency selective hybrid precoding for limited feedback millimeter wave systems," *IEEE Trans. Commun.*, vol. 64, no. 5, pp. 1801–1818, May 2016.
- [15] I. Gupta and A. Ksienski, "Effect of mutual coupling on the performance of adaptive arrays," *IEEE Transactions on Antennas and Propagation*, vol. 31, no. 5, pp. 785–791, Sep 1983.
- [16] C. Masouros, M. Sellathurai, and T. Ratnarajah, "Large-scale MIMO transmitters in fixed physical spaces: The effect of transmit correlation and mutual coupling," *IEEE Trans. Commun.*, vol. 61, no. 7, pp. 2794–2804, July 2013.
- [17] Y. Liu, B. Ai, and B. Chen, "Impact of mutual coupling on LTE-R MIMO capacity for antenna array configurations in high speed railway scenario," in *Proc. VTC (Spring)*, May 2016, pp. 1–5.
- [18] Q. Zhou and X. Ma, "Element-based lattice reduction algorithms for large MIMO detection," *IEEE J. Sel. Areas Commun.*, vol. 31, no. 2, pp. 274–286, February 2013.
- [19] O. H. Toma and M. El-Hajjar, "Element-based lattice reduction aided K-best detector for large-scale MIMO systems," in *Proc. Int. Workshop Signal Process. Adv. Wireless Commun.*, July 2016, pp. 1–5.
- [20] C. Windpassinger and R. F. H. Fischer, "Low-complexity near-maximum-likelihood detection and precoding for MIMO systems using lattice reduction," in *Proc. Inf. Theory and App. Workshop*, March 2003, pp. 345–348.
- [21] A. Lenstra, H. Lenstra, and L. Lovasz, "Factoring polynomials with rational coefficients," *Mathematische Annalen*, vol. 261, no. 4, pp. 515–534, 12 1982.
- [22] E. Agrell, T. Eriksson, A. Vardy, and K. Zeger, "Closest point search in lattices," *IEEE Trans. Inf. Theory*, vol. 48, no. 8, pp. 2201–2214, Aug 2002.
- [23] M. K. Samimi and T. S. Rappaport, "3-D millimeter-wave statistical channel model for 5G wireless system design," *IEEE Trans. Micro. Theory Techn.*, vol. 64, no. 7, pp. 2207–2225, July 2016.
- [24] C. A. Balanis, *Antenna Theory: Analysis and Design*. Wiley-Interscience, 2005.
- [25] B. Clerckx, Y. Zhou, and S. Kim, "Practical codebook design for limited feedback spatial multiplexing," in *Proc. ICC*, May 2008, pp. 3982–3987.
- [26] X. Ma and W. Zhang, "Performance analysis for MIMO systems with lattice-reduction aided linear equalization," *IEEE Trans. Commun.*, vol. 56, no. 2, pp. 309–318, February 2008.
- [27] C. Ling, "On the proximity factors of lattice reduction-aided decoding," *IEEE Trans. Signal Process.*, vol. 59, no. 6, pp. 2795–2808, June 2011.
- [28] P. Silvola, K. Hooli, and M. Juntti, "Suboptimal soft-output MAP detector with lattice reduction," *IEEE Signal Process. Lett.*, vol. 13, no. 6, pp. 321–324, June 2006.
- [29] B. Clerckx, D. Vanhoenacker-Janvier, C. Oestges, and L. Vandendorpe, "Mutual coupling effects on the channel capacity and the space-time processing of MIMO communication systems," in *Proc. ICC*, vol. 4, May 2003, pp. 2638–2642.